Modeling of anomalous electron mobility in Hall thrusters

Justin W. Koo and Iain D. Boyd
Aerospace Engineering Department, University of Michigan, Ann Arbor, Michigan 48104

(Received 23 June 2005; accepted 19 December 2005; published online 10 March 2006)

Accurate modeling of the anomalous electron mobility is absolutely critical for successful simulation of Hall thrusters. In this work, existing computational models for the anomalous electron mobility are used to simulate the UM/AFRL P5 Hall thruster (a 5 kW laboratory model) in a two-dimensional axisymmetric hybrid particle-in-cell Monte Carlo collision code. Comparison to experimental results indicates that, while these computational models can be tuned to reproduce the correct thrust or discharge current, it is very difficult to match all integrated performance parameters (thrust, power, discharge current, etc.) simultaneously. Furthermore, multiple configurations of these computational models can produce reasonable integrated performance parameters. A semiempirical electron mobility profile is constructed from a combination of internal experimental data and modeling assumptions. This semiempirical electron mobility profile is used in the code and results in more accurate simulation of both the integrated performance parameters and the mean potential profile of the thruster. Results indicate that the anomalous electron mobility, while absolutely necessary in the near-field region, provides a substantially smaller contribution to the total electron mobility in the high Hall current region near the thruster exit plane. © *2006 American Institute of Physics*. [DOI: 10.1063/1.2172191]

NOMENCLATURE

μ_e	Electron mobility perpendicular to magnetic field
e	Electron charge
m	Electron mass
ν_m	Electron momentum collision frequency
ν_{neut}	Electron-neutral collision frequency
$\omega_{B,e}$	Electron cyclotron frequency
n_a	Neutral density
n_e	Plasma density
$j_{e,\perp}$	Electron current density perpendicular to magnetic field
$E_\perp$	Electric field perpendicular to magnetic field
p_e	Electron thermal pressure
j_{Hall}	Hall current density
B_r	Radial magnetic field

I. INTRODUCTION

Among the many modeling choices necessary in the computational simulation of Hall thrusters, the modeling of one particular physical phenomenon, the electron mobility, a measure of the response of the electrons to an applied electric field, stands out as a particularly difficult task. This is due to the relative lack of experimental measurements of the electron mobility and an incomplete understanding of the particular physics associated with this phenomenon.

A principal characteristic of Hall thrusters is the relatively high electron current which moves from the cathode towards the anode across the largely radial magnetic field in the acceleration channel. The cathode provides electrons for both the discharges current and to neutralize the plume as shown in Fig. 1. To generate this high electron current observed experimentally, it is necessary in computer simulations to consider an electron mobility perpendicular to the magnetic field, μ_e, that is larger than predicted by classical theory. For the remainder of this paper, the electron mobility perpendicular to the magnetic field is simply referred to as the electron mobility.

Additional electron transport mechanisms have been proposed to reflect this increased electron mobility, but no single mechanism has proved completely successful in modeling the observed behavior of the electron mobility. Since the enhanced electron mobility is so fundamental to thruster operation, it is difficult to isolate its effect experimentally; nevertheless, correctly modeling this additional electron transport mechanism, also known as the anomalous electron mobility, is absolutely critical to the successful numerical simulation of Hall thrusters. In this paper, various computational models and an experimentally motivated electron mobility model are used to simulate a single operating condition of the UM/AFRL P5, a 5 kW laboratory model Hall thruster. Direct comparison between these resulting simulations and experimental performance and potential data is performed to provide insight into the effect of the anomalous electron mobility on simulation fidelity.

II. HALL THRUSTER MODEL

All the computational simulations presented in this paper model a single operating condition of the UM/AFRL P5 Hall thruster running on xenon propellant. Full details of this operating condition are provided in Table I. The computational simulations presented in this paper are produced with a 2D axisymmetric hybrid particle-in-cell Monte Carlo collision (PIC-MCC) Hall thruster code developed by Koo.[1] The physics governing this code is similar to that simulated in codes by Fife[2] and Hagelaar *et al.*[3] In particular, neutrals and ions are modeled with a PIC formulation, while the electron

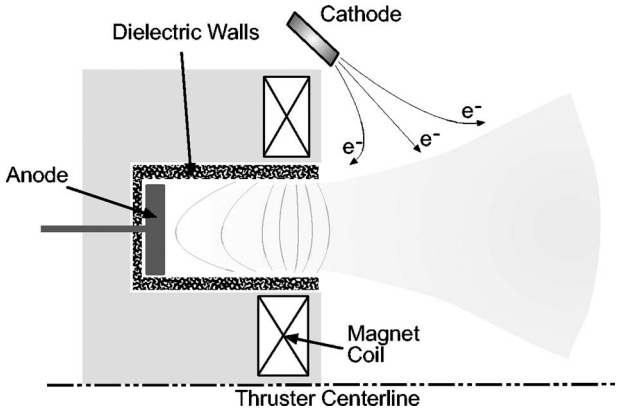

FIG. 1. Dielectric wall Hall thruster schematic. Acceleration channel refers to region bounded by dielectric walls and near field refers to region downstream of thruster face.

fluid is governed by a 1D energy equation assuming isothermal behavior along magnetic field lines. The electrostatic potential is calculated from the thermalized potential via a quasi-1D current conservation approach relying on the magnetic field geometry for spatial discretization. Finally, a MCC algorithm is used to evaluate ionization behavior. The active region of simulation, where the self-consistent electric field and electron energy are evaluated at each time step, measured along the centerline of the thruster acceleration channel is between 0.0104 and 0.078 m from the anode. Upstream of 0.0104 m and downstream of 0.078 m from the anode, Dirichlet boundary conditions for potential (275 and 0 V, respectively) and electron energy (1 and 1 eV, respectively) are enforced.

III. ELECTRON MOBILITY

The classical formulation for electron mobility perpendicular to magnetic field lines is

$$\mu_e = \frac{e}{m\nu_m}\frac{1}{1+\frac{\omega_{B,e}^2}{\nu_m^2}}, \tag{1}$$

where the electron cyclotron frequency is written as

TABLE I. UM/AFRL P5 3.0 kW Xe performance. Cathode mass flow rate: 0.586 mg/s xenon.

	Experimental	Uncertainty
Discharge voltage (V)	300	
Discharge current (A)	10	
Thrust (mN)	180	+1.2/−8
Anode mass flow rate xenon (mg/s)	10.248[a]	
I_{sp} (s)	1744[b]	+20/−131[c]
Efficiency (%)	51	+1/−8.3
Background pressure (Torr)	$1.1\cdot10^{-5}$[d]	

[a]Two-dimensional internal and near-field data taken at 10.736 mg/s.
[b]Actual $I_{sp}=1650$ s presented in Ref. 9 is based on anode plus cathode mass flow rates.
[c]Uncertainty based on $I_{sp}=1650$ s.
[d]Two-dimensional internal and near-field data taken at $3.2\cdot10^{-5}$ Torr.

$$\omega_{B,e} = \frac{eB}{m} \tag{2}$$

and the electron momentum collision frequency, ν_m, considered to be dominated by the electron-neutral collision frequency, is evaluated in similar fashion as Boeuf and Garrigues,[4]

$$\nu_m \approx \nu_{\text{neut}} = 2.5\cdot10^{-13}\times n_a. \tag{3}$$

A. Computational mobility models

A number of models for the anomalous electron mobility have been developed to account for the enhanced electron mobility observed in Hall thrusters. In this work, the various anomalous electron mobility models are assumed to act as additional collision mechanisms and are implemented through augmentation of the electron momentum transfer frequency. The primary computational models for the anomalous electron mobility are now described.

The wall-collision correction to the ν_m term, based on the idea that electrons collide with the sheath with a relative frequency based on their thermal energy and the width of the acceleration channel, has been developed by Boeuf and Garrigues.[4] A simple form for this correction can be obtained by using an *a priori* averaged thermal energy to calculate a global wall-collision rate. For these computations, the modified form of the electron momentum transfer frequency, with wall collisions, where α is an empirically chosen coefficient, is as follows:

$$\nu_m = \nu_{\text{neut}} + \alpha\cdot10^7. \tag{4}$$

The wall-collision approach is based on the theory by Morozov *et al.*[5] that electron-wall collisions are the mechanism for enhancing electron transport inside the thruster. Accordingly, mobility correction is better suited to the acceleration channel (where there are walls) than to the near field of the thruster (where there are no walls). Further theory supporting the contribution of electron-wall collisions to anomalous mobility inside the channel can be found in work by Latocha *et al.*[6]

The Bohm diffusion correction to the ν_m term is based on the idea that anomalous Bohm diffusion results in the additional electron mobility observed experimentally. For these computations, the modified form of the electron momentum transfer frequency, where α_B is an empirically chosen coefficient, is as follows:

$$\nu_m = \nu_{\text{neut}} + \alpha_B\omega_{B,e}. \tag{5}$$

The theory behind the mechanism for Bohm mobility, presented by Esipchuck *et al.*,[7] is based on transport from azimuthal drift waves in the plasma which can exist only in regions with decreasing gradients in the magnetic field. Consequently, the Bohm model for anomalous mobility is less applicable inside the thruster channel where the magnetic field criterion to support these azimuthal drift waves is not met. More recent attempts to identify the physical cause of anomalous transport have focused on the effect of electric field fluctuations in the presence of a crossed magnetic field.

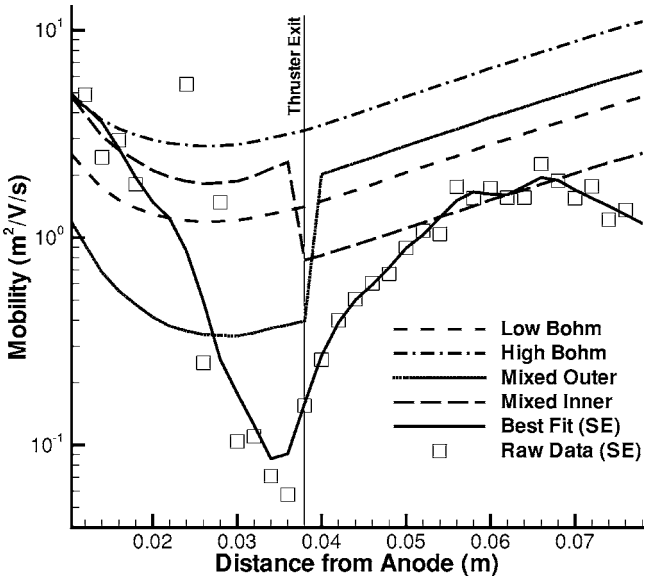

FIG. 2. UM/AFRL P5 mean centerline mobility.

Recent theoretical and computational work by Adams *et al.*,[8] which links anomalous transport to plasma turbulence (through the field oscillations), has yielded some insight into these phenomena, but a general model that can be used within our formulation is not yet available.

To incorporate these ideas, mixed mobility models for Hall thrusters have been presented by Hagelaar *et al.*[3] with a wall-collision mobility model inside the thruster and a Bohm mobility model outside the thruster. The approach used in the present work to blend the two mobility regimes is slightly different than the approach presented by Hagelaar *et al.*;[3] however, the fundamental idea of using wall-collision mobility inside the thruster and Bohm mobility in the near field is identical.

The use of a mixed mobility model, while better capturing the theoretical physics of the problem, introduces extra dimensions to the model parameter space. In this study, the boundary between the two models is fixed at the thruster exit, and two parameters, α inside the channel and α_B outside the channel, are necessary to describe the model.

The anomalous mobility models selected for this section are as follows: (1) Bohm diffusion mobility with $\alpha_B=0.005$ (low Bohm); (2) Bohm diffusion mobility with $\alpha_B=0.015$ (high Bohm); (3) Mixed mobility: wall-collision mobility with $\alpha=0.15$ inside the acceleration channel and Bohm mobility with $\alpha_B=0.020$ outside the channel (mixed outer); and (4) Mixed mobility: wall-collision mobility with $\alpha=5.0$ inside the acceleration channel and Bohm mobility with $\alpha_B=0.008$ outside the channel (mixed inner). Mean centerline electron mobility data for all four models are presented in Fig. 2.

B. Experimental data and semiempirical mobility model

Internal Hall thruster measurements taken by Haas[9,10] provide a substantial dataset of plasma properties inside the UM/AFRL P5 Hall thruster. While not complete enough to generate a completely experimentally based electron mobility profile throughout the device, it does provide most of the information necessary to evaluate the electron mobility. The missing piece of information for this analysis is the electron current density profile. Since the resulting electron mobility profile is only partially based on experimental data, it is referred to in this paper as the semiempirical electron mobility. A detailed formulation of the electron current density profile and the resulting semiempirical electron mobility profile, motivated by work by Meezan,[11] is presented in this section.

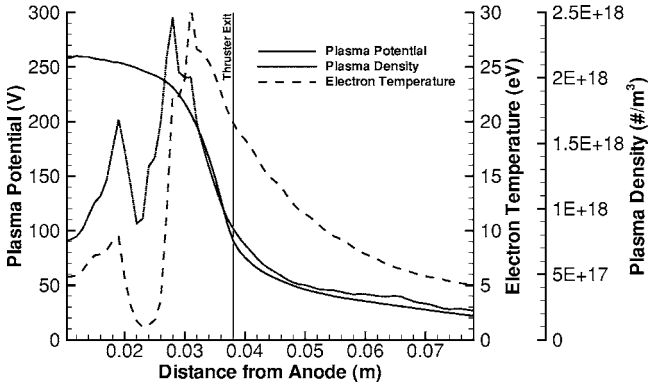

FIG. 3. UM/AFRL P5 plasma properties.

The original experimental data available include axial traces of the plasma potential, electron temperature, and plasma density from 10 to 180 mm from the anode face in 1 mm increments. These data, gathered at 78.5 mm from the thruster centerline, are presented in Fig. 3.

The electron mobility perpendicular to field lines can be formulated as follows:

$$\mu_e = \frac{j_{e_\perp}}{en_e\left(E_\perp + \frac{1}{n_e e}\nabla_\perp p_e\right)}. \tag{6}$$

From this equation, it is clear that the only necessary value which cannot be derived from the available experimental dataset is $j_{e_\perp}$. Since this is a 1D analysis, available experimental data are considered to be constant along radial slices of the simulation. Finally, no time variation is considered in deriving this steady-state mobility profile.

Since the discharge current is fixed through the acceleration channel due to current conservation, an accurate ion current can be used to retrieve the correct electron current. The ion current starts at or near zero (depending on the presence of an anode presheath) at the anode, indicating that the electron current must be equal to (or larger, in the case of an anode presheath) the discharge current at the anode. Since the diameter of the acceleration channel is constant, as the ions are created and accelerated through the thruster, the net ion current density increases and the electron current density decreases correspondingly. A similar process holds in the very near field of the plume as the electron current density diminishes in exact, and opposite, concert with the ion current. Critically, the electron current density, regardless of its magnitude, must remain finite and positive in the region upstream of the effective cathode plane. Any behavior to the

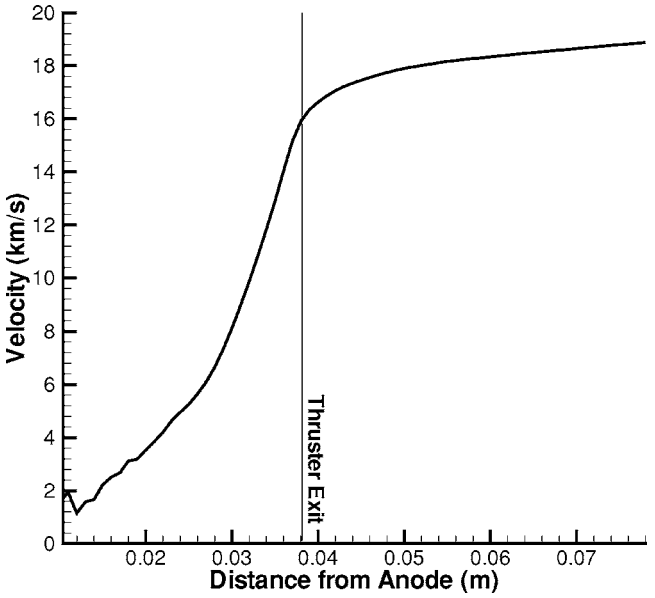

FIG. 4. Idealized ion velocity trace.

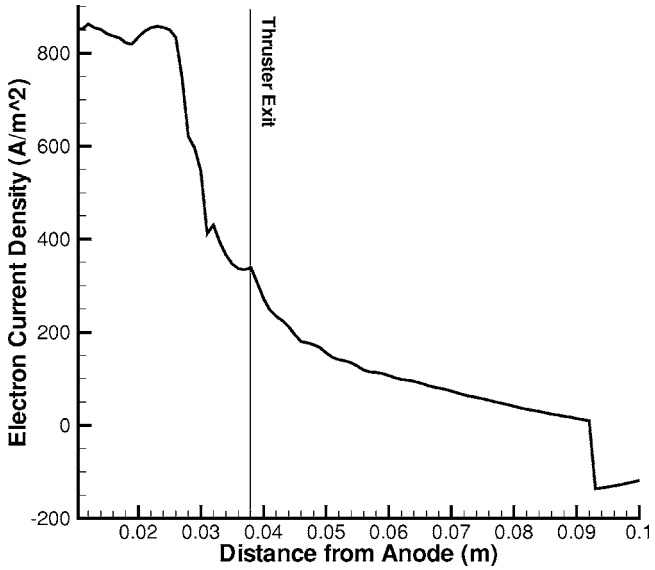

FIG. 5. UM/AFRL P5 electron current density.

contrary implies that the ion current density is actually larger than the discharge current density, which is not a physically acceptable case. At some point further downstream in the plume, the bulk electron motion is no longer upstream towards anode but is now downstream towards the plume as a neutralization source. At this point, since the electrons are now moving away from the thruster instead of towards the thruster, the electron current switches sign from positive to negative.

To determine the ion current density, an idealized ion velocity trace is created which considers the "perfect" acceleration of a singly charged ion from the anode potential to the local thruster potential. The resulting velocity trace is shown in Fig. 4. This assumption is not unreasonable, as the maximum velocity achieved by a singly charged ion assuming perfect acceleration is around 19 km/s, while the thruster exhibits an I_{sp} of around 1750 s, implying an effective propellant exit velocity of around 17.5 km/s.

Although it is theoretically possible to directly calculate the ion current density by the multiplication of the plasma density and the idealized ion velocity trace, since the plasma properties are not radially uniform, the 1D assumption and measurement errors lead to an ion current density which is significantly larger than the discharge current density. The discharge current density is a function of the area of 1D radial slices of the thruster and near-field plume. A 45 deg divergence angle in the near field is considered to evaluate the discharge current density. To compensate for this overestimate, the ion current density is divided by a constant factor to result in a peak ion current density near the effective cathode plane which is only 82% to 92% of the discharge current density. This is the equivalent of selecting an electron current equal to 8% to 18% of the discharge current. Experimental measurements of the UM/AFRL P5 demonstrate that the plasma potential actually rises roughly 5 cm from the thruster exit. Since electric forces, rather than thermal forces, dominate electron motion in this region, the electron current density is likely negative downstream of this potential minimum, which must therefore represent the downstream end of this analysis (the effective cathode plane). The resulting electron current density profile is provided in Fig. 5.

The combination of experimental data and estimated electron current density profile results in the fairly noisy electron mobilities presented in Fig. 2 (negative values are not shown) as the raw data (SE) data points. Since no clear function fits the raw data points and negative values are removed, the data points are fit by hand on a linear-linear plot to a smoothed curve to create the new mobility profile presented in Fig. 2 as the best fit (SE) curve. The best fit curve is implemented in the code by considering the simulation to have a time-independent mobility in the radial direction. Figure 6 provides the raw data points along with the classical electron mobility profile and the Hall current density evaluated as

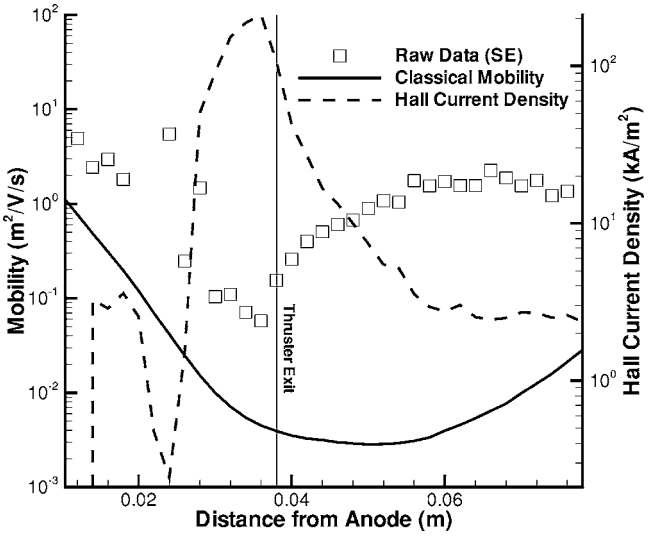

FIG. 6. UM/AFRL P5 centerline properties.

TABLE II. UM/AFRL P5 mobility model performance data.

	Low Bohm	High Bohm	Mixed outer	Mixed inner	Best fit (SE)	Measured
Thrust (mN)	154.5	182.7	169.4	173.9	179.3	180.0
I_{sp} (s)	1544	1824	1686	1728	1792	1744
Ion current (A)	11.07	11.58	9.90	10.92	11.29	N/A
Electron current (A)	0.33	7.41	0.72	2.34	0.05	N/A
Discharge current (A)	11.41	19.00	10.63	13.26	11.34	10.00
Power (W)	3137	5224	2922	3646	3119	3000
Thrust efficiency (%)	37	31	48	40	50	51

$$j_{\text{Hall}} = en_e \frac{E_z}{B_r}. \tag{7}$$

The mobility profiles presented in Fig. 2 represent varying magnitudes of anomalous mobility correction to the classical mobility profile in Fig. 6. In particular, all the mobility models show significant corrections to the classical mobility in the near field of the thruster. The greatest variation between these mobility profiles is in the electron mobility inside the acceleration channel near the thruster exit. As will be shown in the next section, the mobility in this region, typically being lower than anywhere else in the simulation, has a very strong effect on the shape of the potential profile in this crucial region of the thruster.

IV. RESULTS AND COMPARISONS

The integrated performance parameters produced by the four computational mobility models and the best fit curve are shown in Table II. The principal figure of merit for integrated performance data is the thrust. According to this criterion, the high Bohm model, both mixed mobility models, and the best fit curve perform quite successfully. The failing of the low Bohm model is not surprising since it is optimized to the thruster power rather than thrust.

Another important listing in Table II is the electron current. As will become clear in this section, higher mobility coefficients generally result in higher electron currents. Since thrust performance is based largely on the ion current while the thruster power is based on the total current, simulations which produce comparable amounts of thrust can show wide variation in thruster power. In particular, while the high Bohm model provides almost exactly the experimentally observed level of thrust, it overpredicts the required power by over 70%. On the other hand, the mixed outer model underpredicts the experimental thrust by only 6% while maintaining almost exactly the experimental power input. Since the thrust efficiency scales inversely with the discharge current, poor thruster efficiency results when the electron mobility and, consequently, the electron current, is too large. In the best fit case, as a reflection of the extremely low overall electron mobility, the electron current is a tiny fraction of the overall discharge current. Although the semiempirical mobility is based on an assumed 8%–18% electron current fraction at the effective cathode plane, its implementation in a time-dependent 2D code is in a 1D time-independent manner. Consequently, the inability of the code to recover the correct electron current does not represent an unacceptable level of inconsistency.

Although the general trend of higher mobility coefficients corresponding to higher electron currents is generally true, the behavior of this Hall thruster simulation is by no means linear. In particular, although the mixed outer case has a substantially lower mobility inside the thruster than the low Bohm case, it has a higher electron current than does the low Bohm case. From this example, it is clear that the shape of the electron mobility profile, as well as the magnitude, is crucial to determining the physics of the simulation. This is made more clear by the internal and near-field time-averaged centerline plasma potential data presented in Fig. 7.

The low Bohm and high Bohm cases demonstrate the effect of increasing α_B. As desired, when $\alpha_B \cdot \omega_{c,e} \gg \nu_{\text{neut}}$, the correct scaling for μ in the limit of Bohm diffusion, $\mu \propto 1/B$, is reached. Since the α_B correction for the low Bohm case is smaller than for the high Bohm case, the low Bohm mobility case more closely resembles the flatter classical mobility seen in Fig. 6. The effect of the flatter mobility profile in the low Bohm case results in an almost linear potential gradient throughout the acceleration channel. Conversely, greater positive curvature in the electron mobility

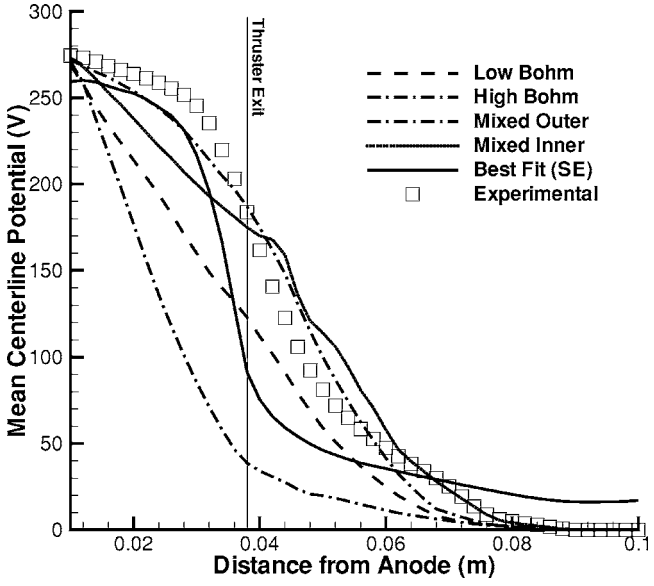

FIG. 7. UM/AFRL P5 centerline plasma potential.

profile is displayed by the high Bohm mobility due to the fairly large corrections to the effective collision rate in regions with small magnetic fields (near the anode and in the near field). Thus, for the high Bohm case, because the mobility drops more quickly in the channel and rises more quickly outside of the channel, the result is a much steeper potential gradient. Although the peak potential gradient is generally close to the minimum in the mobility curve, other factors, such as the electron current, electron temperature, and pressure gradient, couple with the electron mobility to establish a self-consistent potential distribution. As a consequence, even though both Bohm mobility models have their minimum mobility in the same location, the locations of their peak electric fields do not coincide.

The mixed outer case demonstrates the tendency of a high mobility in the near field of the thruster (relative to inside the thruster) to force the acceleration zone into the acceleration channel. The mixed inner case demonstrates the opposite behavior when the near field of the thruster has a low mobility relative to the acceleration channel. By varying the strength of these coefficients, it is possible to control the position of the potential drop relative to the thruster exit. It is not possible, within the framework of this particular implementation, to change the relative shape of the mobility curve beyond the single control parameter (α or α_B) in a given region of the thruster. As a result, for the mixed inner mobility model, the cusp in the mobility profile just upstream of the thruster exit is sufficient to induce a discontinuity in the gradient of the centerline potential just after the thruster exit.

Although the high Bohm potential curve seems to offer fairly close agreement with the experimental potential profile, it cannot provide the same peak electric field magnitude observed experimentally inside the acceleration channel, and especially near the thruster exit region. The peak electric field for this case is actually close to 1 cm beyond the thruster exit rather than right at the thruster exit. Similarly, the mixed inner potential profile, while well representing the potential profile outside the thruster, also provides a peak electric field beyond the thruster exit. Both the low Bohm and mixed outer potential profiles are widely divergent from the experimentally observed data.

The best fit case captures the steepness of the main potential gradient, corresponding to the magnitude of the electric field, in the acceleration channel better than any of the computational mobility models. There remains a serious discrepancy between the value of the experimental potential (180 V) and the best fit potential (90 V) at the thruster exit; however, since this discrepancy does not seem to have an adverse effect on the relative position of the ionization/acceleration zone of the thruster, the integrated performance parameters demonstrate close agreement. Moreover, the 2D potential profiles from the best fit simulation and experimental data presented in Fig. 8 reveal the steepest portion of the potential gradient observed experimentally is fairly close to that predicted by the best fit simulation. Note that the potential "jet" structure observed experimentally has been reproduced recently with a full 2D fluid Hall thruster model by Keidar *et al.*.[12] The inability of the computer simulation to reproduce this feature likely reflects the deficiencies in the quasi-1D formulation rather than in the best fit mobility profile.

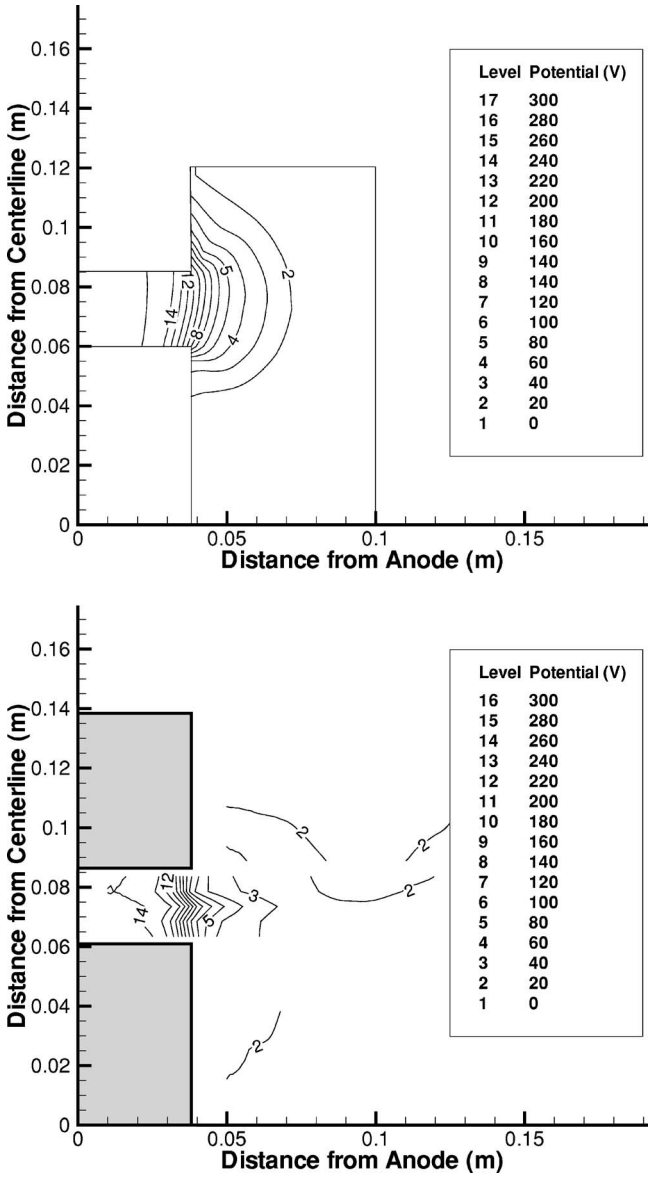

FIG. 8. UM/AFRL P5 mean potential profiles.

From the performance data in Table II and the centerline potential profiles in Fig. 7, it is clear that the existing models for the anomalous mobility can return reasonable integrated performance parameters and potential profiles if tuned appropriately. However, since the semiempirical mobility profile is constructed using the experimental data, it is no surprise that the best fit curve, despite being time independent and purely radial in nature, is able to provide better all-around agreement with the experimental data. It is clear that the shape of the electron mobility profile near the thruster exit plays a substantial role in determining the electric field profile in this region. From Fig. 6, it is clear that this region of high electric field near the exit plane coincides with the region of highest Hall current density. Thus, if the semiempirical electron mobility is accepted as truly representative of the actual electron behavior, then the contribution of the anomalous electron mobility to the true electron mobility diminishes most sig-

nificantly in this high Hall current region, indicating that some feature of the high azimuthal drift is disrupting the anomalous electron transport mechanism. Conversely, it is clear that the use of a Bohm-type correction works well in the near field of the thruster.

V. CONCLUSION

Simulations of the discharge chamber and plume near field of a Hall thruster based on Bohm diffusion and mixed anomalous mobility models reveal that these models can be tuned to provide fairly accurate thrust or discharge current performance; however, it is difficult to match all of the integrated performance parameters simultaneously. With the additional flexibility offered by the mixed mobility models, it is possible to better match the overall integrated performance parameters than with the single coefficient Bohm mobility model; however, since multiple coefficient settings provide fairly realistic solutions, it is not clear which mobility profiles, if any, are physically correct.

To establish an electron mobility profile based on the real electron physics, an experimental dataset was combined with an assumed electron current density profile to create a semiempirical electron mobility profile. This 1D steady-state semiempirical electron mobility profile was smoothed and the resulting "best fit" mobility was used in the computer simulation. Although the best fit mobility profile did not result in a simulation which exactly matched the experimental data, it did provide better overall behavior, in terms of both integrated performance parameters and potential profile, than any of the other anomalous mobility models. Furthermore, the semiempirical electron mobility profile indicated a reduced anomalous mobility contribution to the total electron mobility in the vicinity of the high Hall current region.

ACKNOWLEDGMENTS

The authors gratefully acknowledge financial support from the Air Force Office of Scientific Research through Grant FA9550-05-1-0042.

[1] J. W. Koo and I. D. Boyd, Comput. Phys. Commun. **164**, 442 (2004).
[2] J. M. Fife, Ph.D. thesis, Massachusetts Institute of Technology (1998).
[3] G. J. M. Hagelaar, J. Bareilles, L. Garrigues, and J.-P. Boeuf, J. Appl. Phys. **91**, 5592 (2002).
[4] J. -P. Boeuf and L. Garrigues, J. Appl. Phys. **84**, 3541 (1998).
[5] A. I. Morozov and A. P. Shubin, Sov. J. Plasma Phys. **10**, 728 (1984).
[6] V. Latocha, L. Garrigues, P. Degond, and J. P. Boeuf, Plasma Sources Sci. Technol. **11**, 104 (2002).
[7] Y. V. Esipchuck and G. N. Tilinin, Sov. Phys. Tech. Phys. **21**, 419 (1976).
[8] J. C. Adam, A. Heron, and G. Laval, Phys. Plasmas **11**, 295 (2004).
[9] J. M. Haas, Ph.D. thesis, University of Michigan (2001).
[10] J. M. Haas and A. D. Gallimore, Phys. Plasmas **8**, 652 (2002).
[11] N. B. Meezan, W. A. Hargus, and M. A. Cappelli, Phys. Rev. E **63**, 026410 (2001).
[12] M. Keidar, A. D. Gallimore, Y. Raitses, and I. D. Boyd, Appl. Phys. Lett. **85**, 2481 (2004).